On Radar and Communication Integrated System Using OFDM Signal

Xuanxuan Tian* and Zhaohui Song†
*Shenzhen Graduate School, Harbin Institute of Technology, Shenzhen, China
Email: tianxuanxuan2008@163.com
†School of Information Science and Technology, East China Normal University, Shanghai, China
Email: zhsong@ce.ecnu.edu.cn

***Abstract*—In view of the defects that low data transmission rate and high range sidelobes in radar and communication integrated systems based on traditional orthogonal frequency division multiplexing (OFDM), an OFDM integrated waveform structure and associated processing technique is proposed. Firstly, a phase-coded OFDM (PC-OFDM) integrated waveform based on cyclic shifts of m-sequence is given, where corresponding time shift is controlled by communication data. Then, the radar processing technique based on discrete Fourier transform (DFT) and correlation is analyzed in detail. Theoretical analysis and simulation results show that the proposed method can achieve joint high-resolution range and velocity estimation of the target under high data transmission rate.**

I. Introduction

Recently, radar and communication integrated systems using common waveforms for simultaneously performing radar and communication function on general hardware platforms are popular [1], the study on radar and communication integration is to improve spectrum efficiency and cost effectiveness. A typical application scenario for such systems would be in the unmanned aerial vehicle (UAV) formation flight system, which demands the ability of inter-UAV communication as well as reliable environment sensing.

Orthogonal frequency division multiplex (OFDM) signal takes advantages of high range resolution, simple realization, good antimultipath performance, etc. which has been widely applied in radar and communication systems. A multicarrier complementary phase-coded (MCPC) signal based on OFDM-coded construction was proposed by Levanon [2], [3]. The main idea of information encoded and phase modulated subcarriers to achieve radar and communication functions appeared in [4]. In subsequent years, radar and communication integration based on OFDM signals has received more and more attentions.

When considering the present research related to radar processing approaches in the integrated systems, a classical approach of direct match filtering by calculating correlation of the transmitted and received signals was presented in Ultra Wideband OFDM integrated system [5]. One subcarrier carried 1 bit of information, and was aimed at application for targets at short ranges. However, high range sidelobes were easily produced. The system performance was unreliable for carrying arbitrary communication data.

A modulation symbol-based processing approach for Range-Doppler estimation had been proposed in OFDM integrated system for vehicular applications [1], [6]. It removed completely the influence of communication data, and the range resolution was generally in the order of 1 to 2 m, but ambiguities might be produced due to the improper subcarrier separation.

An adaptive pulse compression (APC) approach to improve detection performance for OFDM integrated system was presented in [7], it introduced a very high computational effort for using the cyclic iterative algorithm. OFDM Linear Frequency Modulation (OFDM-LFM) integrated signal based on Fractional Fourier Transform (FRFT) was proposed in [8]. LFM signal experienced Range-Doppler coupling, the accuracy of velocity compensation was of great importance on range estimation.

A pulse compression method based on fast Fourier transform (FFT) for PC-OFDM radar signal was introduced [9], which was mathematically equal to match filtering. A synthetic filtering method based on FFT and decoding to obtain the high resolution range profile was proposed in [10], [11]. Azimuth processing based on multiple signal classification (MUSIC) algorithm for multiple-input-multiple-output (MIMO) OFDM radar system was proposed in [12], but these did not consider the effect of communication information on radar processing.

In view of the above, we use the carried data bit to control the time-shift of phase-coded (PC) sequence in PC-OFDM integrated signal, and take full usage of the signal structure to get high resolution range-velocity profile of target. The rest of this paper is organized as follows. In section II, the form of PC-OFDM integrated waveform and the construction method for PC sequences are presented. In section III, the radar processing approach is given. The simulation results are presented in section IV. Conclusion of the paper is given in section V.

978-1-4673-8823-8/17/$31.00 ©2017 IEEE

II. Waveform Structure

A. Waveform of PC-OFDM Integrated Signal

PC-OFDM signal consists of N subcarriers transmitted simultaneously, the binary data carried each subcarrier is mapping onto a sequence of M bits. Refer to [11], PC-OFDM integrated signal can be written as

$$s(t) = \sum_{p=0}^{N_p-1} \sum_{n=0}^{N-1} \sum_{m=0}^{M-1} w_n a_{pnm} \text{rect}(t - pT_r - mT_c - T_c/2) \times \exp\left[j2\pi f_n (t - pT_r)\right] \tag{1}$$

where N_p is the number of pulses, N is the number of subcarriers, M is the number of chips, w_n is the nth subcarrier weight, T_r is the pulse repetition period, T_c is the chip duration, $\Delta f = 1/T_c$ is subcarrier separation, $f_n = n\Delta f$ is the nth subcarrier frequency. rect(t) is given by

$$\text{rect}(t) = \begin{cases} 1 & -\frac{T_c}{2} \le t \le \frac{T_c}{2} \\ 0 & otherwise \end{cases} \tag{2}$$

a_{pnm} is the phase code of the nth subcarrier, the mth chip and the pth pulse, assuming that $a_{pnm} = a_{nm}$, this means PC sequences per pulse is identical. PC sequences is represented as S given by

$$S:\ a_{nm}, \quad n = 0, \ldots, N-1,\ m = 0, \ldots, M-1 \tag{3}$$

B. Construction of PC Sequences

In this paper, assuming that $N = M$ and the choice of N is a power of 2. m-sequence and its cyclic shifted versions having an ideal periodic autocorrelation function has been shown in [13], which is here put into a formal proof. The construction for PC sequences is based on cyclic shifts of m-sequence, and the corresponding time shift is controlled by communication data. Specific construction steps are summarized as follows.

1) Generate the initial PC sequence $\mathbf{m}$. m-sequence of length $N-1$ and its ending by zero-padding can be written as $\{m'_n\}_{n=0}^{N-1}$, $m'_n \in \{0, 1\}$, which is represented bipolar bits as $\mathbf{m}$ given by

$$\mathbf{m} = \{m_n\}_{n=0}^{N-1}, \quad m_n \in \{-1, 1\} \tag{4}$$

2) Randomly generate the transmitted communication data $\mathbf{d}$ in decimal format. $K = \log_2 N$ data bits carried on the nth subcarrier can be expressed as $\{b_n(k)\}_{k=0}^{K-1}$, $b_n(k) \in \{0, 1\}$, which converts into decimal form d_n, this represents the corresponding time shift for the nth subcarrier. The time shifts for all subcarriers can be expressed as

$$\mathbf{d} = \{d_n\}_{n=0}^{N-1} \tag{5}$$

3) Cyclic shift. $\mathbf{m}_{\to d_n}$ is the PC sequence on the nth subcarrier that represents cyclically shifted $\mathbf{m}$ by d_n. Hence, the PC sequences can be written as

$$S = \begin{bmatrix} \mathbf{m}_{\to d_0} \\ \mathbf{m}_{\to d_1} \\ \vdots \\ \mathbf{m}_{\to d_{N-1}} \end{bmatrix} \tag{6}$$

III. Processing Scheme

In the following we take into account the radar processing on the PC-OFDM integrated signal, an approach based on DFT and correlation similar to the algorithm described in [11] is chosen. The complete processing scheme is shown in Fig. 1, the details of these steps are illustrated as follows.

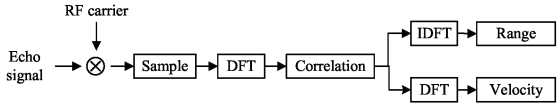

Fig. 1: Processing scheme block diagram

A. Baseband Received Signal

The received echo signal is to demodulate by multiplying radio frequency (RF) carrier frequency, so the baseband received signal in a noise-free scenario can be written as

$$\begin{aligned} r(t) &= \sum_{k=1}^{N_t} \sigma_k s(t - \tau_k) \exp(-j2\pi f_c \tau_k) \\ &= \sum_{k=1}^{N_t} \sum_{p=0}^{N_p-1} \sum_{n=0}^{N-1} \sum_{m=0}^{M-1} \sigma_k w_n a_{nm} \\ &\quad \times \exp[j2\pi f_n (t - \tau_k - pT_r)] \exp(-j2\pi f_c \tau_k) \\ &\quad \times \text{rect}(t - \tau_k - pT_r - mT_c - T_c/2) \end{aligned} \tag{7}$$

where

$$\tau_k = 2(R_k - V_k t)/c \tag{8}$$

where N_t is the number of targets, f_c is the RF carrier frequency, c is the speed of light in free space, σ_k is the scattering coefficient of the kth target, R_k and V_k are the initial distance and relative velocity between the kth target and radar, respectively. Assuming that $V_k > 0$ when the target is fleeing from the radar, and meeting $2V_k/c \ll 1$.

B. Sample

Sampling frequency of D/A converter is $f_s = N/T_c$, sampling time is $t = pT_r + mT_c + iT_c/N$, $p = 0, \ldots, N_p - 1$, $m = 0, \ldots, M-1$, $i = 0, \ldots, N-1$. $r(t)$ in sampled version can be written as

$$\begin{aligned} r(p, m, i) = &\sum_{k=1}^{N_t} \sum_{n=0}^{N-1} \sigma_k w_n a_{nm} Q_1(k, n) Q_2(p, m, k, n) \\ &\times \exp(j2\pi F_n \frac{iT_c}{N}) \end{aligned} \tag{9}$$

where

$$Q_1(k,n) = \exp[-j2\pi(f_c + f_n)\frac{2R_k}{c}] \tag{10}$$

$$Q_2(p,m,k,n) = \exp[j2\pi(f_c + f_n)\frac{2V_k}{c}(pT_r + mT_c)] \tag{11}$$

$$F_n = (f_c + f_n)\frac{2V_k}{c} + f_n \tag{12}$$

C. DFT

The transform from received signal samples $r(p,m,i)$ to frequency-domain signal by applying DFT concerning i can be written as

$$R'(p,m,q) = \sum_{i=0}^{N-1} r(p,m,i)\exp(-j2\pi\frac{i}{N}q)\ q = 0,\ldots,N-1 \tag{13}$$

Substituting (9) into (13), we get

$$R'(p,m,q) = X(p,m,q) + \varepsilon(p,m,q) \tag{14}$$

where

$$\begin{aligned} X(p,m,q) =& \sum_{k=1}^{N_t} \sigma_k w_q a_{qm} Q_1(k,q) Q_2(p,m,k,q) \\ &\times \mathrm{Comb}(\eta) \end{aligned} \tag{15}$$

$$\begin{aligned} \varepsilon(p,m,q) =& \sum_{k=1}^{N_t}\sum_{n=0,n\neq q}^{N-1} \sigma_k w_n a_{nm} Q_1(k,n) Q_2(p,m,k,n) \\ &\times \mathrm{Comb}(\eta + n - q) \end{aligned} \tag{16}$$

and

$$\mathrm{Comb}(\eta) = \frac{\sin(\pi\eta)}{\sin(\pi\eta/N)}\exp[j\pi\eta(\frac{N-1}{N})] \tag{17}$$

and

$$\eta = \frac{2V_k}{c} f_c T_c \tag{18}$$

$\varepsilon(p,m,q)$ destroys the orthogonality of subcarriers and results in inter-carrier interference. For the low-speed targets, $\varepsilon(p,m,q)$ can be negligible [11]. Hence, (14) can be rewritten as

$$R'(p,m,q) = X(p,m,q) \tag{19}$$

D. Correlation Processing

The correlation processing between $R'(p,m,q)$ and the PC sequence on the qth subcarrier can be expressed as

$$\begin{aligned} D(p,j,q) =& \sum_{k=1}^{N_t} \sigma_k w_q Q_1(k,q)\mathrm{Comb}(\eta) \\ &\times \exp[j2\pi(f_c + f_q)\frac{2V_k}{c} pT_r] A_q(j) \end{aligned} \tag{20}$$

where

$$\begin{aligned} A_q(j) =& \sum_{m=0}^{M-1-|j|} a_{qm} a^*_{q(m+|j|)} \exp[j2\pi(f_c + f_q)\frac{2V_k}{c} mT_c] \\ &|j| = 0,\ldots,M-1 \end{aligned} \tag{21}$$

Obviously, (21) contains the autocorrelation function(ACF) of PC sequence on the qth subcarrier, this results in one single peak. Hence, the peak value of $D(p,j,q)$ with respect to j can be expressed as

$$\begin{aligned} D_{max}(p,q) =& \sum_{k=1}^{N_t} \sigma_k w_q A_{qj} Q_1(k,q)\mathrm{Comb}(\eta) \\ &\times \exp[j2\pi(f_c + f_q)\frac{2V_k}{c} pT_r] \end{aligned} \tag{22}$$

where

$$A_{qj} = \max|A_q(j)| \quad |j| = 0,\ldots,M-1 \tag{23}$$

A_{qj} is the energy of the PC sequence of the qth subcarrier, which is known after PC sequence is chosen. Hence, removing w_q and A_{qj}

$$Y(p,q) = \frac{D_{max}(p,q)}{w_q A_{qj}} \tag{24}$$

which can be rearranged into

$$\begin{aligned} Y(p,q) =& \sum_{k=1}^{N_t} \sigma_k \mathrm{Comb}(\eta) \\ &\times \exp[-j2\pi(f_c + q\Delta f)\frac{2R_k}{c}] \\ &\times \exp[j2\pi(f_c + q\Delta f)\frac{2V_k}{c} pT_r] \end{aligned} \tag{25}$$

From above formula, it contains the range and velocity information. Therefore, it must be possible to estimate range and velocity independently through a suitable processing approach.

E. Range Estimation by IDFT

Range estimation can be obtained by taking the inverse discrete Fourier transform (IDFT) of $Y(p,q)$ concerning q

$$y(p,l) = \frac{1}{N}\sum_{q=0}^{N-1} Y(p,q)\exp(j2\pi\frac{q}{N}l) \quad l = 0,\ldots,N-1 \tag{26}$$

which can be calculated and simplified as

$$\begin{aligned} y(p,l) =& \sum_{k=1}^{N_t} \sigma_k \mathrm{Comb}(\eta)\frac{\sin[N\pi(\Delta f\tau_k - l/N)]}{\sin[\pi(\Delta f\tau_k - l/N)]} \\ &\times \exp[-j2\pi f_c\tau_k - j\pi(N-1)(\Delta f\tau_k - l/N)] \end{aligned} \tag{27}$$

As can be seen from (27), under the condition

$$\Delta f\tau_k - l/N = \pm h \quad h = 0,1,2\ldots \tag{28}$$

$|y(p,l)|$ gets its peak value. If accumulating time is short, namely, $R_k \gg V_k p T_r$, we can get

$$R_k \approx \frac{(\pm h + l/N)c}{2\Delta f} \tag{29}$$

F. Velocity Estimation by DFT

Velocity estimation can be obtained by taking DFT of $Y(p,q)$ concerning p

$$y(\nu,q) = \sum_{p=0}^{N_p-1} Y(p,q)\exp(-j2\pi\frac{p}{N_p}\nu) \quad \nu = 0,\ldots,N_p-1 \tag{30}$$

which can be calculated and simplified as

$$\begin{aligned} y(\nu,q) =& \sum_{k=1}^{N_t} \sigma_k \mathrm{Comb}(\eta) Q_1(k,q) \\ &\times \frac{\sin[N_p\pi(\frac{T_r(f_c+f_q)2V_k}{c} - \frac{\nu}{N_p})]}{\sin[\pi(\frac{T_r(f_c+f_q)2V_k}{c} - \frac{\nu}{N_p})]} \\ &\times \exp[j\pi(N_p-1)(\frac{T_r(f_c+f_q)2V_k}{c} - \frac{\nu}{N_p})] \end{aligned} \tag{31}$$

As can be seen from (31), under the condition

$$\frac{T_r(f_c+f_q)2V_k}{c} = \frac{\nu}{N_p} \tag{32}$$

$|y(\nu,q)|$ gets its peak values, hence

$$V_k = \frac{\nu c}{2N_p T_r(f_c+f_q)} \tag{33}$$

From the above, we can see that the complete radar processing contains a few key steps. Firstly, the baseband received signal after demodulation to get frequency-domain signal by applying DFT. Secondly, correlation processing with the transmitted PC sequences is performed. Thirdly, high resolution range estimation is obtained by applying IDFT. Finally, high resolution velocity estimation is obtained by applying DFT. Hence, the complete process can be implemented through digital signal processing (DSP), and it is crucial to study the digitization of radar system.

IV. Simulation and Analysis

Simulations are carried out to demonstrate the performance of the system, the details of the system parameters are summarized in Table I. We use randomly generated communication data of size $(128 \times \log_2 128)$ and m-sequence of length 127 to construct the integrated signal, adding in additive white Gaussian noise (AWGN), and assuming that $\sigma_k = 1$ and $w_n = 1$.

TABLE I
OFDM SYSTEM PARAMETERS

Symbol	Parameter	Value
f_c	Carrier frequency	10GHz
N_p	Number of pulses	64
N	Number of subcarriers	128
M	Number of chips	128
T_c	Chip duration	0.2us
T	Pulse width	25.6us
T_r	Pulse repetition period	0.1ms
δ	Pulse duty cycle	0.256
Δf	Subcarrier separation	5MHz
B	Total signal bandwidth	640MHz
ΔR	Range resolution	0.23m
ΔV	Velocity resolution	2.34m/s
SNR	Signal-to-Noise ratio	10dB

A. Radar Performance

1) Performance Comparison : Simulations are carried out to evaluate the two targets with $R_1 = 12004\mathrm{m}$, $R_2 = 12005\mathrm{m}$, $V_1 = 45\mathrm{m/s}$, $V_2 = 60\mathrm{m/s}$. The results based on the proposed radar processing method and the classic match filtering are shown in Fig. 2 and Fig. 3, respectively.

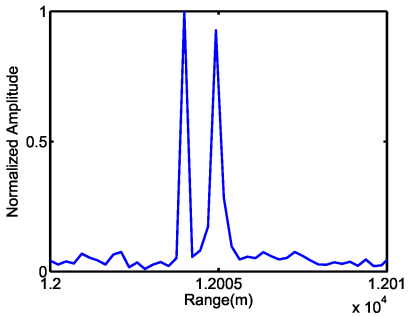

(a) Range profile

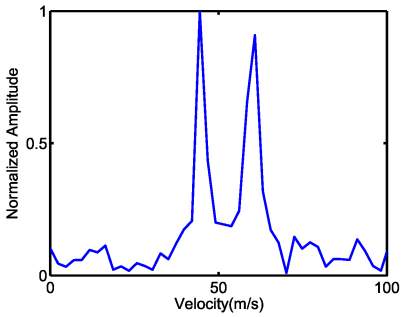

(b) Velocity profile

Fig. 2: Test result for two targets with $R_1 = 12004\mathrm{m}, \mathrm{R}_2 = 12005\mathrm{m}, \mathrm{V}_1 = 45\mathrm{m/s}, \mathrm{V}_2 = 60\mathrm{m/s}$

Fig. 2(a) and (b) illustrate the range profile and velocity profile respectively. It can be seen that the two targets can be

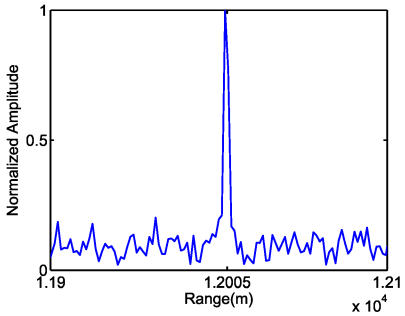

Fig. 3: Range profile based on matched filtering

TABLE II
TARGETS SETTING PARAMETERS

Setting	$\mathbf{R_1[m]}$	$\mathbf{R_2[m]}$	$\mathbf{V_1[m/s]}$	$\mathbf{V_2[m/s]}$
1	12005	12005.3	50	50
2	12005	12005.2	50	50
3	12005	12005	50	53
4	12005	12005	50	52

separated successfully. The estimated ranges and velocities are 12003.98m, 12004.92m, 44.44m/s, 60.82m/s, respectively. As shown in Fig. 3, there exists one single peak that can not identify the two adjacent targets. The results demonstrate the performance advantage of the proposed processing approach through numerous numeric results.

2) Resolution : In order to evaluate the effectiveness of the proposed algorithm concerning the achievable resolution on the separability of adjacent targets. The detected range and velocities for targets are as summarized in Table II, and the corresponding range profile and velocity profile are shown in Fig. 4 and Fig. 5, respectively.

As shown in Fig. 4, the two targets in a distance difference of $\Delta d = 0.3\text{m}$ are separable, but not of $\Delta d = 0.2\text{m}$. As shown in Fig. 5, the two targets in a velocity difference of $\Delta v = 3\text{m/s}$ are separable, but not of $\Delta v = 2\text{m/s}$. That is because that two targets must be a distance minimum of $\Delta R = 0.23\text{m}$ and a velocity minimum of $\Delta V = 2.34\text{m/s}$ apart to be successfully resolved in this simulation. Hence, the simulation results verify that the proposed processing approach is able to detect multiple adjacent targets.

3) Effect of Velocity on Range Estimation : In order to verify the effect of velocity on the range estimation is tested for one single target with $R = 12005\text{m}$ at the different velocity $V = (100\text{m/s},\ 2000\text{m/s},\ 5000\text{m/s})$. As shown in Fig. 6, the peak values are located at 12004.92m, 12004.22m, 12003.05m, respectively. Therefore, it can be seen that range slightly decreases for the high-velocity target, and range estimation is under little influence of the velocity. This is an advantage for PC-OFDM radar signal, and has already been shown in [14].

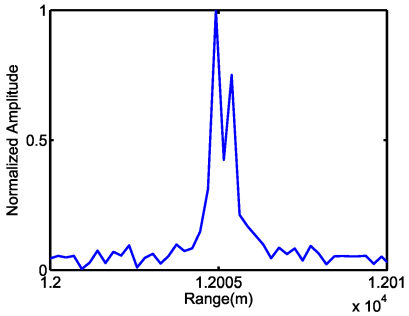

(a) $\Delta d = 0.3\text{m}$

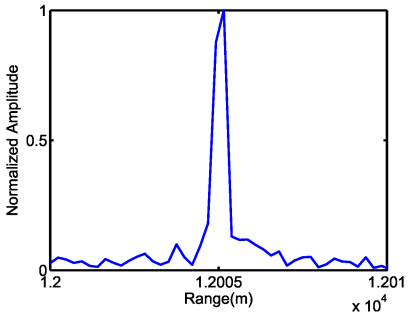

(b) $\Delta d = 0.2\text{m}$

Fig. 4: Range profile for setting 1&2

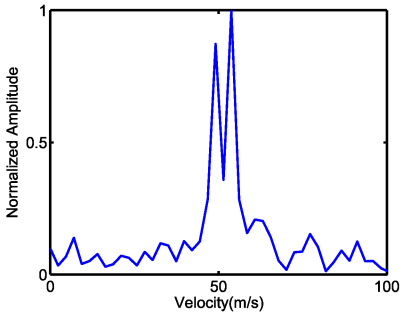

(a) $\Delta v = 3\text{m/s}$

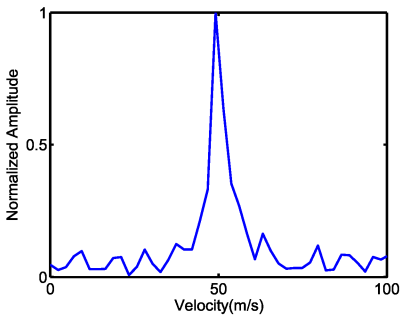

(b) $\Delta v = 2\text{m/s}$

Fig. 5: Velocity profile for setting 3&4

B. Communication Performance

For the integrated signal, each subcarrier carries $\log_2 N$ bits of information, each pulse can transmit $N \times \log_2 N$ bits.

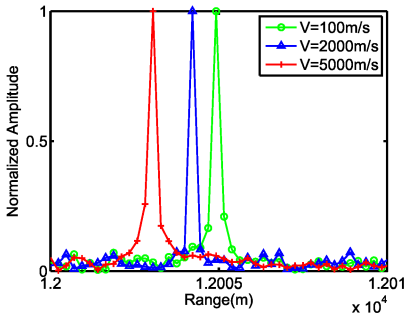

Fig. 6: Range profile for a target with $R = 12005\text{m}$ at different velocity

Hence, the data transmission rate can be calculated as

$$\frac{128 \times \log_2 128}{25.6} \times 0.256 = 8.96\text{Mbps} \tag{34}$$

from the above equation, it can meet the requirements of transmitting mass data in a short time [15].

Fig. 7 shows the simulation results of bit error rate (BER) for different data transmission rate tests. It can be seen that BER becomes better as SNR increases, and a larger data transmission rate results in a poorer BER. Hence, BER and data transmission rate need to be taken into account in the design of system.

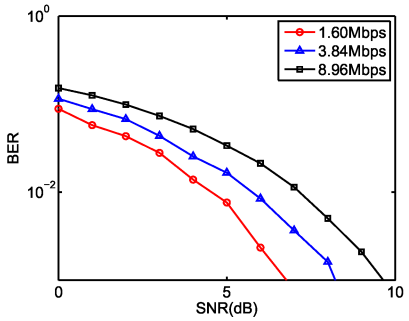

Fig. 7: BER for different data transmission rate

V. Conclusion

In this paper, we have presented and analyzed a radar and communication integrated system based on PC-OFDM signal. The form of the integrated signal and the associated construction of PC sequences are given. The radar processing method is then presented. From theoretical analysis and simulation results, we can get the following observations, (i) every subcarrier carries $\log_2 N$ data bits for the integrated signal, thus resulting in a high data transmission rate, but a larger data transmission rate results in a worse BER. (ii) The radar processing algorithm can obtain the joint high-resolution estimation of ranges and velocities for adjacent targets. These conclusions and presented method can provide insights to the design and operation of radar and communication integrated system.

Acknowledgment

This work was sponsored by the National Science Foundation of China (91638204) and Shenzhen Fundamental Research Project (JCYJ20160318094236224).

References

[1] C. Sturm and W. Wiesbeck, "Waveform design and signal processing aspects for fusion of wireless communications and radar sensing," *P. IEEE.*, vol. 99, no. 7, pp. 1236–1259, 2011.

[2] N. Levanon, "Multifrequency complementary phase-coded radar signal," *IEE P-RADAR SON NAV.*, vol. 147, no. 6, pp. 276–284, 2000.

[3] E. Mozeson and N. Levanon, "Multicarrier radar signals with low peak-to-mean envelope power ratio," *IEE P-RADAR SON NAV*, vol. 150, no. 2, pp. 71–77, 2003.

[4] B. Donnet and I. Longstaff, "Combining MIMO radar with OFDM communications," in *Proc. EuRAD '06*, Manchester, UK, Sep. 13–15, 2006, pp. 37–40.

[5] D. Garmatyuk, J. Schuerger, Y. T. Morton, K. Binns, M. Durbin, and J. Kimani, "Feasibility study of a multi-carrier dual-use imaging radar and communication system," in *Proc. EuRAD '07*, Munich, Germany, Oct. 10–12, 2007, pp. 194–197.

[6] Y. L. Sit, L. Reichardt, C. Sturm, and T. Zwick, "Extension of the OFDM joint radar-communication system for a multipath, multiuser scenario," in *Proc. IEEE RadarCon '11*, Kansas, USA, May 23–27, 2011, pp. 718–723.

[7] M. Ruggiano, E. Stolp, and P. V. Genderen, "Multi-target performance of LMMSE filtering in radar," *IEEE Trans. Aerosp. Electron. Syst.*, vol. 48, pp. 170–179, Jan. 2012.

[8] K. Chen, Y. Liu, and W. Zhang, "Study on integrated radar-communication signal of OFDM-LFM based on FRFT," in *Proc. IET Radar '15*, Hangzhou, China, Oct. 14–16, 2015, pp. 1–6.

[9] R. Mohseni, A. Sheikhi, and M. A. M. Shirazi, "A new approach to compress multicarrier phase-coded signals," in *Proc.IEEE RadarCon '08*, Rome, Italy, May 26–30, 2008, pp. 1–6.

[10] B. Deng, X. Wei, and X. Li, "Pulse compression technique for multi carrier phase-coded radar," in *Proc. ICSPS'10*, vol. 1, Dalian, China, Jul. 5–7, 2010, pp. 329–332.

[11] K. Huo, B. Deng, Y. Liu, W. Jiang, and J. Mao, "High resolution range profile analysis based on multicarrier phase-coded waveforms of OFDM radar," *J SYST ENG ELECTRON*, vol. 22, no. 3, pp. 421–427, Jun. 2011.

[12] Y. L. Sit, C. Sturm, J. Baier, and T. Zwick, "Direction of arrival estimation using the MUSIC algorithm for a MIMO OFDM radar," in *Proc. IEEE RadarCon '12*, Atlanta, USA, May 7–11, 2012, pp. 0226–0229.

[13] B. M. Povovic, "Complementary sets based on sequences with ideal periodic autocorrelation," *Electron. Lett.*, vol. 26, no. 18, pp. 1428–1430, 1990.

[14] G. Franken, H. Nikookar, and P. Van Genderen, "Doppler tolerance of OFDM-coded radar signals," in *Proc. EuRAD '06*, Manchester, UK, Sep. 13–15, 2006, pp. 108–111.

[15] L. Hu, Z. Du, and G. Xue, "Radar-communication integration based on OFDM signal," in *Proc. ICSPCC'14*, Guilin, China, Aug. 5–8, 2014, pp. 442–445.